ACS APPLIED MATERIALS & INTERFACES

Research Article

www.acsami.org

Engineering Functionality Gradients by Dip Coating Process in Acceleration Mode

Marco Faustini,[†] Davide R. Ceratti,[†] Benjamin Louis,[†] Mickael Boudot,[†] Pierre-Antoine Albouy,[‡] Cédric Boissière,[†] and David Grosso*[,†]

[†]Sorbonne Universités, UPMC Univ Paris 06, CNRS, Collège de France, UMR 7574, Chimie de la Matière Condensée de Paris, F-75005 Paris, France

[‡]Univ Paris 11, CNRS, UMR8502, Lab Phys Solides, F-91405 Orsay, France

Supporting Information

ABSTRACT: In this work, unique functional devices exhibiting controlled gradients of properties are fabricated by dip-coating process in acceleration mode. Through this new approach, thin films with "on-demand" thickness graded profiles at the submillimeter scale are prepared in an easy and versatile way, compatible for large-scale production. The technique is adapted to several relevant materials, including sol–gel dense and mesoporous metal oxides, block copolymers, metal–organic framework colloids, and commercial photoresists. In the first part of the Article, an investigation on the effect of the dip coating speed variation on the thickness profiles is reported together with the critical roles played by the evaporation rate and by the viscosity on the fluid draining-induced film formation. In the second part, dip-coating in acceleration mode is used to induce controlled variation of functionalities by playing on structural, chemical, or dimensional variations in nano- and microsystems. In order to demonstrate the full potentiality and versatility of the technique, original graded functional devices are made including optical interferometry mirrors with bidirectional gradients, one-dimensional photonic crystals with a stop-band gradient, graded microfluidic channels, and wetting gradient to induce droplet motion.

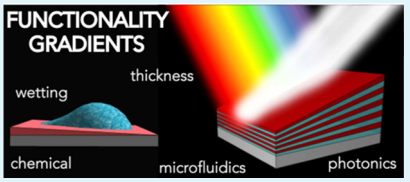

KEYWORDS: *thin films, gradient, dip-coating, photonics, wetting*

1. INTRODUCTION

Functionality gradients can be found in many natural systems. For instance, the cactus plants developed an efficient method to collect water from environmental fog based on wetting gradients in their spines.[1] In eye optics, gradients in refractive index allow focusing with good resolution and low aberration at both short and long distances.[2] In the same way, artificial graded surfaces and materials can be engineered to induce properties variation and development of advanced devices for many technological domains such as for controlled wetting, combinatorial studies, tunable optics, aerospace, and so forth. In the literature, wetting lateral gradients are certainly the most popular and most described systems.[3] Several examples on the preparation of chemical gradients were based on selective functionalization by natural diffusion of a chemical agent[4−6] or by controlled immersion in a solution.[7] Similarly, chemical gradients in silica films were obtained by varying the solution composition during dip-coating,[8−10] while other graded systems were developed by exploiting the natural diffusion/sedimentation of colloids in a liquid medium to build, for instance, optical devices.[11] Wetting gradients were also spatially tuned by varying surface topography, but these are quite cumbersome to prepare since specific patterning techniques, such as lithography or selective electrochemical etching/deposition,[12−14] are required. On the other hand, being able to prepare thin films with thickness gradients could potentially enlarge their application field. The deposition of thin films with controlled thickness gradient at submillimeter scale is far from being an easy task and this aspect has been barely addressed in the literature. Among the deposition techniques, one of the most serious candidates is the dip-coating process. This technique is very popular, both in research and development and in production, since it is simple, scalable on large surfaces and it was adapted for the deposition of a great number of different materials of the three main families (organic, ceramic, metals) such as polymers, sol–gel, colloids, hybrids, and so forth.[15,16] More importantly, dip coating deposition permits a high degree of control on thickness and structure through the mastering of the withdrawal speed and of all the evaporation-related parameters (environmental temperature and atmosphere).[17] In particular, in a conventional dip-coating process, the substrate is withdrawn from a solution at a constant speed and the final film has a thickness that depends on the value of the latter withdrawal speed, with a homogeneity that depends on the stability of the speed. Landau and Levich[18] first developed an equation to describe this thickness/speed relationship, and this model was further implemented and adapted by other groups.[17,19,20] However, while the effect of withdrawal speed is now well understood and even predicted, the influence of acceleration in the dip-coating process remains

Received: July 20, 2014
Accepted: August 22, 2014
Published: August 22, 2014

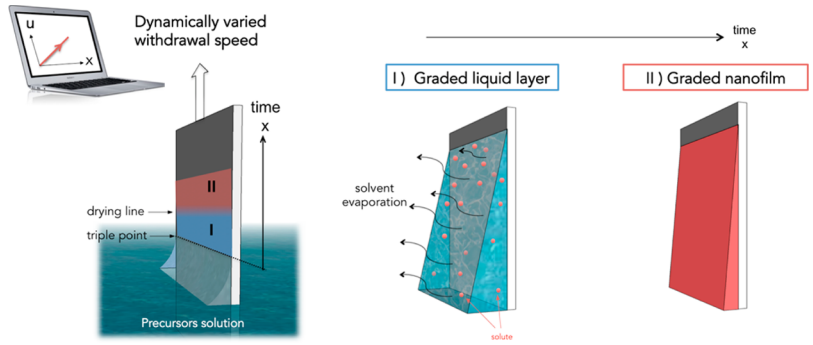

Figure 1. Schematic representation of the dip-coating deposition process in acceleration mode for the formation of controlled graded nanofilms. Two zones are identified: zone I, graded liquid layer below the drying line; zone II, graded nanofilm above the graded line.

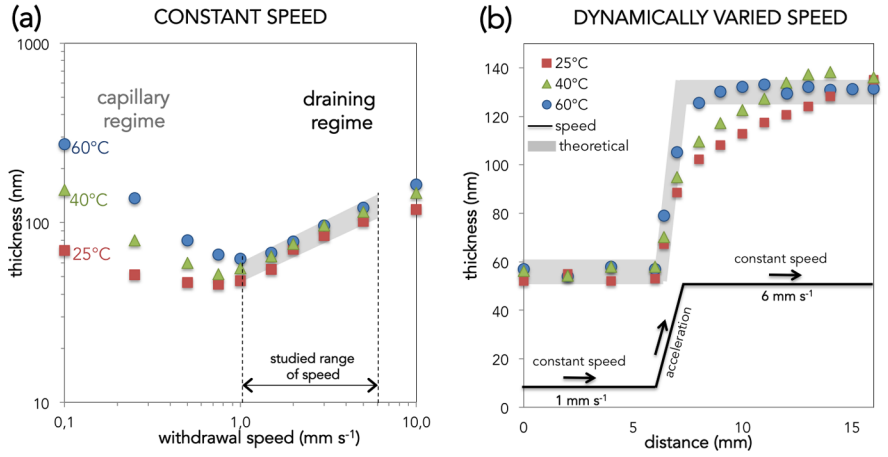

Figure 2. Effect of evaporation rate on graded nanofilms obtained by dip coating process in acceleration mode using mesoporous TiO_2 films as model system. The concentration of the solution in nonvolatile precursors is equal to 3.9×10^{-4} mol cm^{-3}. (a) Plot of the experimental and predicted values of thickness versus withdrawal speed of homogeneous nanofilms obtained by conventional constant speed dip coating at different temperatures; (b) plot of the experimental and theoretical values of thickness as a function of the distance of the graded films obtained by dip-coating in acceleration mode at different temperatures.

a black box. This is particularly interesting since the dynamic variation of the dipping rate during dip coating can theoretically allow the deposition of films with variable thickness along the dipping direction. Very recently, a parametric study showed the feasibility of a similar approach but applied to a horizontal flow-coating process and only limited to polymer coatings.[21] In this work, we demonstrate that dip-coating process can be performed in acceleration mode to obtain graded films and to generate devices with controlled functionality gradients. In the first part of the Article, we investigate, for the first time, the effect of the acceleration in the dip coating process, describing the potentialities and limitation of this approach. In particular, the influence of the speed variation on the thickness profiles is studied together with the important roles played by the evaporation rate and by the viscosity on the fluid draining-induced film formation. We demonstrate that, starting from semiexperimentally established relations used to predict thickness in constant regimes, on-demand thickness profiles can be prepared. The approach can be generalized to several relevant materials, including sol–gel dense and mesoporous metal oxides, block copolymers, metal–organic framework colloids, and commercial photoresists. In the second part, we describe how dip-coating in acceleration mode can be used to induce controlled variation of functionalities by playing on structural, chemical, or dimensional variations. The versatility of the process is demonstrated here by several examples of unique graded functional devices such as (i) optical multilayers interferometry mirrors/filters with bidirectional gradients, (ii) one-dimensional (1D) photonic crystals with a stop-band gradients, (iii) microfluidic channels with gradient in height, and (iv) surfaces with wetting gradient to induce droplet motion. Thin layer structure and properties were characterized by SEM-FEG, spectroscopic ellipsometry, fluorescence microscopy, and contact angle measurements.

2. RESULTS AND DISCUSSION

2.1. Acceleration in Dip-Coating Deposition Process.

In the conventional dip-coating process, the substrate is dipped into the solution and withdrawn at a constant speed, typically between 1 and 10 mm s^{-1} in the Landau–Levich draining regime. A thin layer of solution is pulled out from the reservoir thanks to surface wetting and draining, while evaporation turns it into a homogeneous dried solid film. The thickness of the initial liquid layer, and thus of the final film, is adjusted by the withdrawal speed.[18] Intuitively, one would expect to be able to tune the thickness into preprogrammed gradients, or into more complex thickness profiles, by just playing on the withdrawal speed modulation. In the present investigation, we decided to address thickness gradients achieved through controlled acceleration modes. To do so we used the commercial dip-coating equipment "ACEdip" from Solgelway, which allows speed profile programing along the withdrawal direction (x)

with a minimal increment down to 0.01 mm and a precision as small as 0.0005 mm s^{-1}. Such characteristics are important so as to be able to decorrelate the fluid inertia from the mechanical motion inertia. The latter dip-coater is also equipped with an atmosphere and temperature controlled environmental chamber to ensure controlled evaporation and reproducibility. Different speed variation profiles can be settled in order to obtain graded thin films as illustrated in Figure 1.

The substrate is withdrawn from the precursor solution at increasing speeds. Two zones in the time/space domain can be identified in the scheme in Figure 1. First, a graded liquid layer is formed between the triple-phase line and the drying line in zone I, where evaporation of the volatile species is active.[19] The length of zone I can be reduced or enlarged by tuning the evaporation rate with the temperature or/and the relative vapor pressure in the chamber. Zone II is located above the drying line and represents the graded solid thin film composed of the nonvolatile species. The resulting films can be eventually further stabilized and processed by thermal treatment such as in the case of sol–gel based materials.[19] In order to evaluate the influence of the speed variation and the degree of control in the formation of such graded layers, a parametric study was performed. Sol–gel derived, mesoporous titania films were chosen as model system because of their great importance in many application domains such as photocatalysis,[22] sensors,[23] or dye-sensitized solar cells.[24,25] As "fresh" sol–gel films obtained just after dip-coating are highly sensible to atmospheric conditions and their thickness can considerably be modified by a slight change in temperature and humidity, the samples were stabilized by heat treatment at 500 °C for 5 min.

The final thickness and refractive index of calcined films were measured by spectroscopic ellipsometry. Plots of the film thickness measured after stabilization versus withdrawal speed (constant regime) for three different temperatures are reported in Figure 2a. Influence of the main chemical and processing critical parameters, together with the related mechanisms have been described in our previous report.[17] Briefly, for all the dipping temperatures, two distinct regimes of deposition are visible for both speed extremities, while the minimal thickness is obtained for an intermediate regime. The "capillary regime" of deposition is found at speed below 0.1 mm s^{-1}. In these conditions, the deposition is governed by the convective hydrodynamic flow induced by the faster evaporation at the triple-phase line. Evaporation rate is thus a key parameter that needs to be controlled by modulating the environmental temperature, as clearly shown in Figure 2a. Thicker films are thus obtained by increasing the temperature in the chamber. An intermediate regime is located between 0.1 and 1 mm s^{-1}, where the minimal thickness is obtained.

The "draining regime" corresponds to the conventional range of withdrawal speeds (>1 mm s^{-1}) where the thickness/speed dependence is fairly well described by the classical Landau–Levich model,[18] that relies on the gravity induced viscous drag opposing the adhesion of the fluid on the substrate. It predicts that the equilibrium thickness depends on the density, the surface tension, and the viscosity of the fluid and is proportional to the withdrawal speed at the power 2/3. As opposed to the capillary regime, the temperature in the chamber does not significantly affect the final thickness. The general semi-experimental relationship (1) has been established in order to link the final thickness (h) to the solution chemical and processing conditions.[17]

$$h = k(Eu^{-1} + Du^{2/3}) \quad (1)$$

The term k is the material volume proportion constant that accounts for the final film structure, porosity, and composition, which are both related to the initial solution. k is thus fixed for a defined solution. The capillary regime of deposition is associated with the first term (Eu^{-1}), where E is the evaporation rate and u is the withdrawal speed, while the viscous drag regime of deposition is associated with the second term of deposition ($Du^{2/3}$), where $\langle\langle D\rangle\rangle$ represents the global constant, and it is related to the physicochemical constants of the solution as described by the Landau–Levich model.[18] As already described in a previous article, the global costant $\langle\langle D\rangle\rangle$ could be determined semiempirically from some thickness measurements of films obtained in the draining regime.[17] The equation and the table with the experimental values are reported in Supporting Information S1 and Table S1.

The following study of the effect of the withdrawal speed concerns the speed range from 1 to 6 mm s^{-1}, where the capillarity term (Eu^{-1}) can be neglected as clearly deduced from Figure 2a. The first experiment consisted of three step profile dip-coating speed conditions, as shown in Figure 2b. The first step, consisting of a constant speed at 1 mm s^{-1}, is followed by a second step where speed is linearly increased from 1 and 6 mm s^{-1} on 1 mm distance. Finally, a constant speed of 6 mm s^{-1} is maintained as the third step. In this range of speeds, where the capillary contribution can be neglected, the theoretical final thickness of the film at a position (x) is calculated using eq 2:

$$h(x) \cong kD[u(x)]^{2/3} \quad (2)$$

In acceleration mode, eq 2 can be written as a function of the speed variation du/dx as follows:

$$h(x) = kD\left[u_0 + \frac{du(x)}{dx}x\right]^{2/3} \quad (3)$$

where u_0 is the initial withdrawal speed since the speed variation du/dx is equal to 5 s^{-1} in the present experiment, and knowing the value of kD extracted form the slope in Figure 2a, one can predict the theoretical final thickness of the films for each value of x. Because kD does not significantly differ when temperature is increased from 25 to 60 °C (see the gray band in Figure 2a), a similar thickness variation prediction can be done in this range of temperature in acceleration mode. Figure 2b first shows that the experimental thicknesses obtained between 25 and 60 °C deviated from the theoretical values, especially in the later part of the acceleration zone. The thickness profiles indicate that the experimental points eventually meet the theoretical values calculated for the fixed final speed of 6 mm s^{-1}. At 25 °C, 8 mm distance from the speed stabilization position at 6 mm s^{-1} is required. These 8 mm can be deduced as being the draining distance or the distance of vertical displacement of the liquid phase before it becomes viscous enough to resist gravity. In addition, this deviation from theoretical tendency is greater at 25 °C than at 60 °C, where a much better correspondence is found. Here, it is clear that the evaporation rate plays an important role in the formation of such graded films in acceleration mode. The deviation from prediction is due to a draining-induced-thickness-shift effect that is present in all dip-coated systems. A schematic explanation of this effect is illustrated in Supporting Information Scheme S1. As already mentioned, the graded

liquid layer (zone I) is simultaneously subjected to draining and to evaporation, with both effects tending to decrease the solution layer thickness. The length of zone I depends thus on the time required to dry the layer, and it tends to decrease when the speed is low (thinner liquid layer) and when the evaporation rate is high. Indeed, a faster evaporation rate allows a faster increase of the viscosity and thus a much lower draining contribution, resulting a much lower deviation as experimentally observed in Figure 2b. One observes here that the deduced draining distance reduces to 5 mm at 40 °C and to 2 mm at 60 °C, confirming thus the latter hypothesis. Therefore, considering the illustration of Figure 1, one must account for the latter deviation in order to better adjust deposition conditions and achieve desired thickness gradients. It is clear that a higher temperature is preferred to reduce the draining distance and to have a more straightforward relation between u and h in speed variation modes, when the system allows it.

The potentials and limitations of such approach were verified by similar experiments that were carried out at 60 °C, by varying the speed variation du/dx and the solution concentration. Figure 3a shows the plot of the predicted and

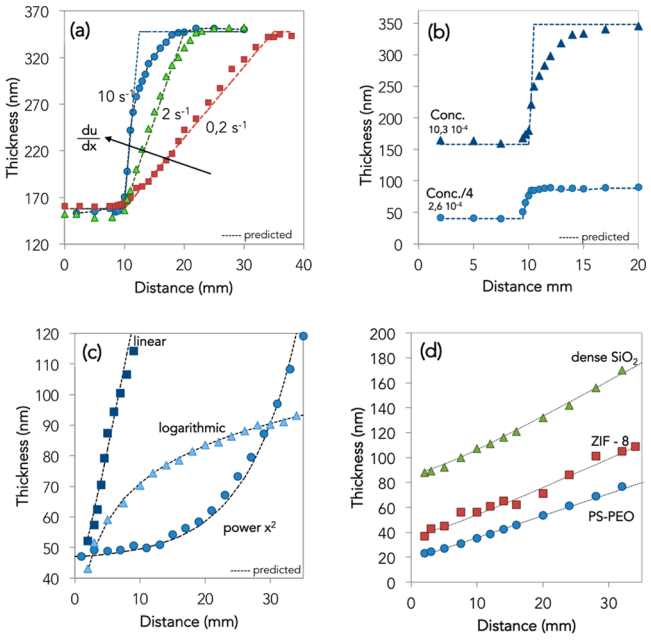

Figure 3. (a) Plot of the thickness of graded mesoporous TiO_2 films for different acceleration rates applied between 1 and 6 mm s^{-1}. (b) Effect of the dilution: plot of the thickness of graded mesoporous TiO_2 films from solution with two different concentrations (10.3 and 2.6 × 10^{-4} mol cm^{-3} in nonvolatile species) and speed variation between 1 and 6 mm s^{-1}. (c) Thickness of graded mesoporous TiO_2 films for linear, logarithmic, or square power profiles. (d) Plot of the thickness of linear graded films of dense SiO_2, of colloidal ZIF-8, and of block copolymer PS-*b*-PEO. All the experiments were conducted by dip-coating at 60 °C.

experimental thickness profiles of the graded mesoporous TiO_2 films obtained from a more concentrated solution (10.3 × 10^{-4} mol cm^{-3}) and for speed variations ranging from 0.2 to 10 s^{-1}. While a fairly good correspondence is found at 0.2 s^{-1}, the deviation in thickness profiles from prediction is observed for increasing speed variation values. This is in agreement with the previous investigation since a faster increase of speed would create a greater difference in draining distance and, therefore, a higher deviation from the theoretical thickness. Figure 3b displays plots of the thickness of graded mesoporous TiO_2 films prepared at 10 s^{-1} from the same solution as in Figure 3a but with different dilutions (1/1 and 1/4).

While a relevant deviation from prediction was observed at high concentration, a good correspondence is found for the diluted system. These results can be explained by the combined effect of the viscosity and evaporation rate for concentrated solutions. Indeed, dip-coating from concentrated systems lead to thicker liquid films that will take a longer time to evaporate. In addition, it is well-known by Raoult's law that the evaporation rate of a solution decreases with the solute concentration. In general, from concentrated systems, it will be more difficult to deal with higher speed variation values that require shorter evaporation times. All these considerations are valid for accelerating systems; however, the prediction and the control of the thickness profile are more complex in the case of deceleration. This is an important aspect that is beyond the scope of this Article, and that will be addressed in future works.

The full control of the processing parameters allows fabrication of on-demand thickness profiles. Withdrawal speed profiles $u(x)$ can be programmed by inverting eq 2 as follows:

$$u(x) = \left[\frac{h(x)}{Dk_i}\right]^{3/2} \tag{4}$$

Figure 3c displays the experimental and predicted values of thickness of graded films following linear, logarithmic, or square power increases of thickness along the dipping distance from an initial withdrawal speed of 1 mm s^{-1}. The approach was also generalized to other systems as shown in Figure 3d where linear graded films where made from (i) sol–gel derived silica, (ii) colloidal metal–organic framework ZIF-8, (iii) and PS-*b*-PEO block copolymer.

In particular, making gradients of the latter organic PS-*b*-PEO is very valuable, for instance, for the investigation of thickness-dependent self-assembly in solvent annealing processes.[26] Other relevant examples of systems with graded functionalities will be shown in the following sections. The fabrication of these systems was performed by dip-coating in optimized conditions for gradients, following the considerations reported in this first part.

2.2. Functional Graded Materials. *2.2.1. Bidirectional Optical Gradients in Multilayers.* Multistack systems with bidirectional graded optical properties can be used for rapid combinatorial investigations of the structural versus optical properties in the case of Bragg reflectors, waveguides, antireflective coatings,[27] and so forth. In addition to theoretical predictions, this experimental approach is very powerful for the development of new devices. Potentially, the characterization of one single graded system can replace the multitude of individual samples prepared with constant thickness (prepared by spin-coating for instance). One example is shown in Figure 4. The optical system is prepared by multistep dip-coating deposition and is composed of four layers, alternating low refractive index mesoporous SiO_2 and high refractive index dense TiO_2 films. Between each dip-coating, the layers were prestabilized at 130 °C for 30 min in order to consolidate the silica network without decomposition of the organic template, avoiding by this way its extraction and replacement by titania precursors through capillary infiltration upon the successive dipping/withdrawal sequences. A final thermal treatment at 450 °C for 15 min in air allowed the decomposition of the template,

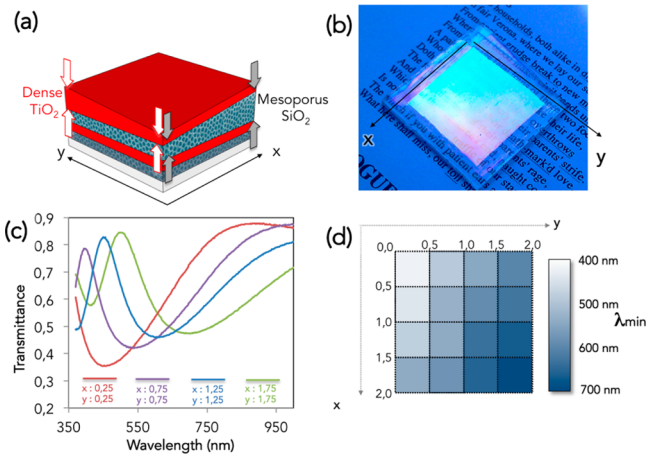

Figure 4. (a) Illustration of the reflective multistack dense TiO_2/mesoporous SiO_2 with bidirectional double gradients. (b) Optical photograph of the multistack applied on glass. (c) UV–vis normal transmission spectra of the multistack system taken in different places in the x–y plane (values of coordinate in centimeters). (d) Mapping of the wavelength of minimal transmission in the x–y plane.

creating the mesoporosity, and the consolidation of SiO_2 and TiO_2 networks (TiO_2 crystallizes into Anatase nanoparticles in such conditions).[23,28] The refractive index values at 700 nm were measured to be 1.35 for the SiO_2 based layers and 2.1 for the TiO_2 layers. The thicknesses of the first two bottom layers are kept constant and equal to 67 and 60 nm for the silica and titania films, respectively. Linearly graded films were then applied on the top of the latter two first layers by dip-coating at 60 °C in acceleration mode. The first layer had a gradient thickness in the x direction and the second one in the y direction as illustrated in Figure 4a, which was made possible by rotating the sample of 90° between each deposition. The preparation process and the values of thickness versus dipping distance in x and y directions for the SiO_2 and TiO_2 films are reported in Supporting Information Figure S1.

The optical photo of the 2 × 2 cm^2 size multilayers applied on glass substrate is displayed in Figure 4b. The device is working as a reflector where the reflected structural colors result from the constructive interferences of light. The presence of graded layers induces bidirectional gradients in structural reflected colors that are clearly visible from the optical image. The optical response of the bidirectional graded systems was evaluated by transmission spectra taken at normal incidence in several x–y coordinates. The size of the light spot for this investigation was reduced to less than 1 mm in order to minimize the effect of thickness variation of graded films. Figure 4c shows some representative transmission spectra taken along the diagonal as indicate by x–y coordinates (in cm). Mapping of the wavelength of minimal transmission in the x–y plane is shown in Figure 4d. In this case, the variation of the high or low index layer thicknesses allows tuning the intensity and the wavelength of the reflection in the visible range from 400 to 730 nm. This simple example demonstrates how bidirectional gradients in multilayers can be used for fast combinatorial investigation of the optical properties that can be directly linked to the layers structure and to the processing conditions.

2.2.2. One-Dimensional Photonic Crystal with Graded Photonic Stop-Band. One-dimensional photonic crystals are usually multilayered systems with a spatial periodicity in their dielectric constant. They are widely used as mirrors, laser cavities, optical filters, and sensors and for mirror shade

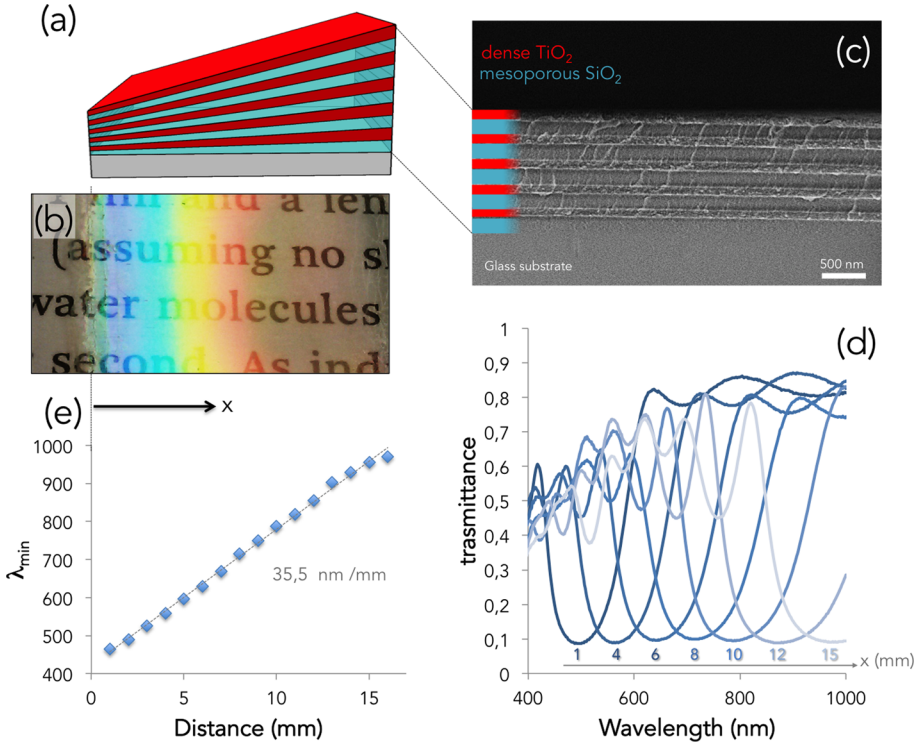

Figure 5. (a) Illustration of the graded 1D photonic crystal. (b) Optical photograph of graded 1D photonic crystal on glass substrate. (c) SEM-FEG micrograph of the five pair system taken at distance x = 16 mm. (d) UV–vis transmission spectra of the graded photonic crystal for increasing x values. (e) Plot of the photonic stop-band position as a function of distance in the x-direction.

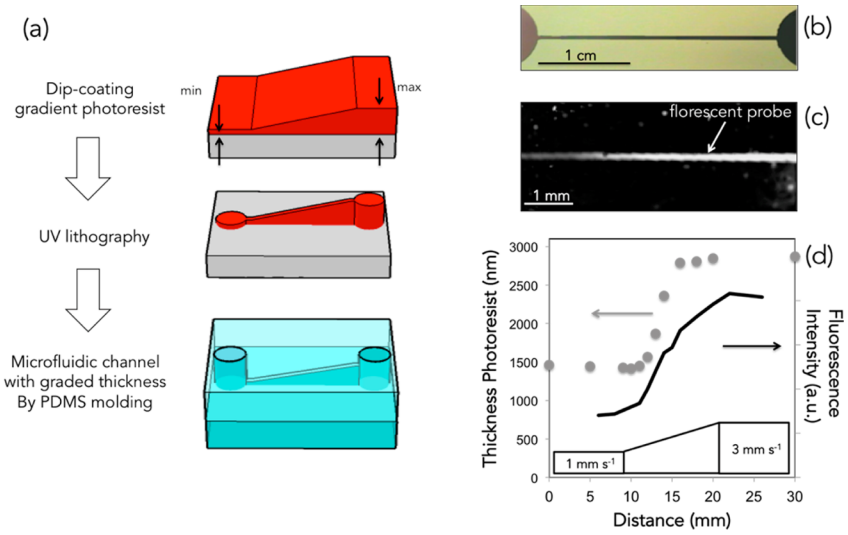

Figure 6. (a) Illustration of process for the fabrication of the graded microfluidic device. (b) Optical photograph of the graded patterned photoresist master. (c) Fluorescence microscopy image of the graded microfluidic channel filled with a fluorescent probe. (d) Plots of thickness of the photoresist layer and fluorescent intensity as a function of the distance.

sunglasses. These systems are able to inhibit the propagation of certain light wavelengths, giving rise to structural color as in the case of butterfly wings. The photonic stop-band position depends on optical thicknesses of the two components. In here, we exploit the potential of dip-coating in acceleration mode in order to fabricate, for the first time, 1D photonic crystals exhibiting a controlled lateral gradient in photonic stop-band. The graded device is illustrated in the scheme in Figure 5a. The system is made of five pairs of alternated low and high refractive index layers based on mesoporous SiO_2 and dense TiO_2 (following the protocol reported in section 2.2.1). Both materials have been processed in order to obtain linear gradients along a distance of 16 mm. The thicknesses after thermal treatment at 450 °C were evaluated by ellipsometric analyses and ranged from 71 to 161 nm for the SiO_2 layers and from 55 to 124 nm for TiO_2 ones. A cross-sectional view of the multistack at a dipping distance equal to 16 mm is displayed in the SEM micrograph in Figure 5c. The optical device on glass substrate acts as a graded reflector as demonstrated by the optical photograph in Figure 5b.

In particular, Figure 5d shows the transmission data of the systems taken at various dipping distance x as indicated by the arrow. Interestingly, the photonic stop-band can be displaced over a very wide range of wavelengths without variation in the minimum transmittance values (less that 10%). The plot of stop-band minimum wavelength versus dipping distance is shown in Figure 5e. A good linear relationship is found with an increase in the position of the minimal transmitted wavelength of 35 nm mm^{-1}, and this from 470 to 960 nm. These results indicate that this kind of device can be potentially used as versatile optical filter or mirror in which the stop-band position can be easily tuned from UV to the IR domains (depending on the absorption limits of all components) by simply displacing the light beam position over the surface.

2.2.3. Microfluidic Channel with Height Gradient. Graded thin films can be further processed through conventional lithographic techniques for the preparation of graded patterns. This is particularly promising for example in microfluidics for the fabrication of channels with gradient in height, not achievable by previously reported protocols. The more conventional and cost-effective strategy for fabricating microfluidic devices is based on PDMS replication from a rigid master obtained by UV lithography. The initial master with the desired microfluidic pattern is generally made by deposition of a photoresist layer on a substrate that is patterned by UV exposure through a specific mask.[29] By this approach, a very high degree of complexity can be achieved in the design of channels in the two lateral dimensions. However, since the photoresist thickness is normally constant, the fabrication leads to microfluidic devices with channels having constant height. Being able to master the photoresist thickness profile allows tuning the channel's height in the same device and increasing its complexity in the third dimension. This aspect can open a wide range of perspectives for size-dependent combinatorial experiments,[30] for sorting, concentration, or manipulation of objects including immiscible droplets.[31,32]

The experimental protocol toward graded channels is illustrated in Figure 6a. A conventional negative photoresist is deposited on the silicon substrate by dip-coating in acceleration mode. The dipping speed profile and the thickness values measured by ellipsometry are reported in the plot of Figure 6d. The withdrawal speed was varied from 1 to 3 mm s^{-1}, resulting in a linear variation of the thickness from 1.5 to 2.8 μm.

The sample was UV-patterned in order to obtain a single linear channel of around 150 μm in width. The graded microfluidic device was prepared by further PDMS molding and bonding. The transfer of the gradient was demonstrated by capillary infiltration of an aqueous solution containing a fluorescent probe in the channel as displayed in the fluorescence microscopy image of Figure 6c. The fluorescent intensity along the channel is plotted in Figure 6d; the fluorescent intensity profile is in good agreement with thickness profile of the initial photoresist. This simple proof-of concept is a demonstration on effectiveness of the approach that could be further implemented to design customized height profiles in microchannels.

2.2.4. Wettability Gradient for Droplet Motion. In this experiment, the surface is engineered in order to induce the spontaneous motion of a water droplet by the presence of a gradient of contact angle and thus of wettability.[5] The key idea

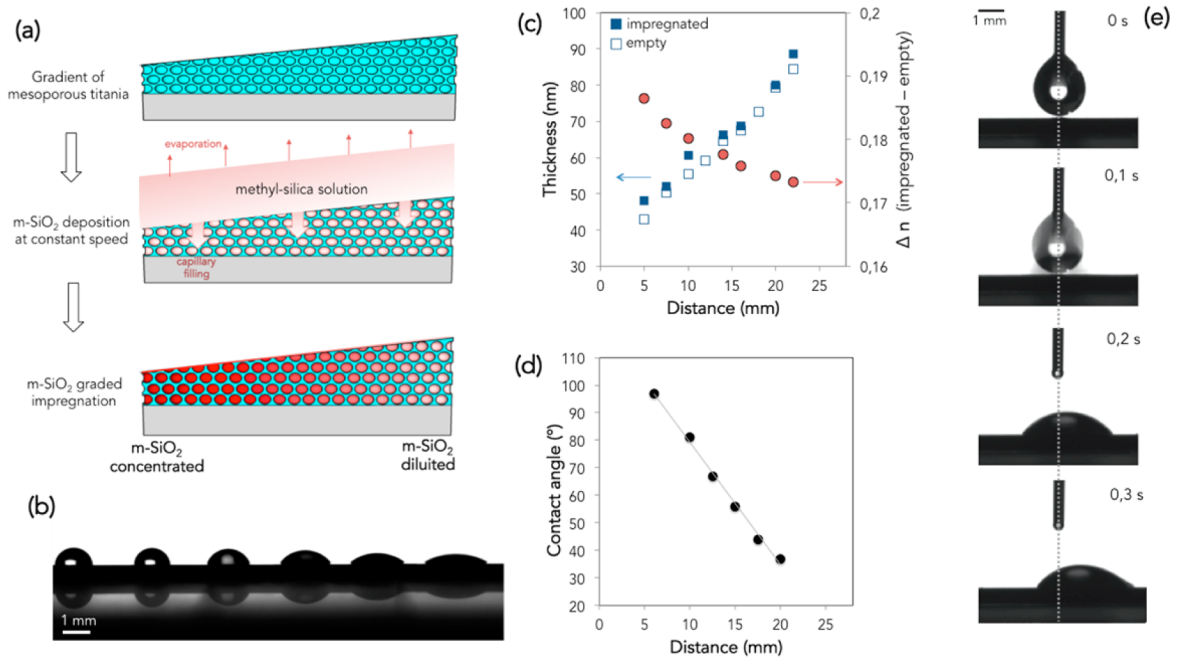

Figure 7. (a) Illustration of the strategy for the preparation of the surface with wettability gradient. (b) Optical image of water droplet at different distance from contact angle device. (c) Plot of the thickness of the mesoporous layer before and after impregnation as a function of the gradient distance; plot of the difference in refractive index between the impregnated and empty layer as a function of the gradient distance. (d) Plot of the contact angle values as a function of the gradient distance. (e) Sequence of optical images of a droplet motion on the wettability graded surface.

consists of creating a composition gradient in the layer without affecting the structure and the optical transparence of the coating: the fabrication protocol is illustrated in Figure 7a.

A superhydrophilic mesoporous TiO_2 film was prepared by dip-coating in order to obtain a linear gradient of thickness from 42 to 83 nm. This porous system is used as reservoir to be impregnated with hydrophobic methylated silica species (m-SiO_2). The infiltration is made by dip-coating at constant withdrawal speed from a diluted ethanol-based solution containing the precursors following a procedure similar to what was already reported for other materials.[33−35] When the sample is dipped into the m-SiO_2 solution, the porosity is immediately filled by the precursor solution. Upon withdrawal, a liquid layer containing the precursor is deposited on the mesoporous TiO_2 substrate. Three distinct phenomena occur: (i) the evaporation of the volatile solvent that leads to the decrease of the thickness of liquid layer with an increase of the precursor concentration; (ii) the drag of the remaining concentrated solution into the mesoporosity by capillarity filling; (iii) complete evaporation of the solvent and deposition of m-SiO2 species into the pores. In this configuration, the amount of m-SiO_2 precursor solution applied per unit surface is constant. Since the thickness of the porous TiO_2 reservoir varies over the surface, a gradient in m-SiO_2 concentration into the pores is expected, building up a gradient in hydrophobic m-SiO_2/hydrophilic TiO_2 fraction. After evaporation, the system was thermally treated at 450 °C for 5 min in order to stabilize the hybrid hydrophobic silica phase.[27] The effectiveness of the impregnation was evaluated by ellipsometry. The plot in Figure 7c indicates that the thickness profile of the "empty" system (only TiO_2) corresponds with the impregnated one (composite m-SiO_2/TiO_2) meaning that no excess of material was deposited on the top of the surface. Another information can be deduced from the difference in refractive index between the empty and the impregnated system (Δn). This value can be seen as a difference in optical density of the film and used to evaluate the effective amount of m-SiO_2 infiltrated into the porosity. As reported in plot of Figure 7c, the Δn is decreasing with the distance corroborating the presence of m-SiO_2 concentration gradient in the film. The latter results were confirmed by contact angle measurement over the surface. An optical image of 1 μL water droplets lying on the film at different distance is shown in Figure 7b while the correspondent average values of contact angle are displayed in the plot of Figure 7d. The wettability varies linearly along the surface with the contact angle values ranging from 98 to 35°. The linear variation can be quantified being equal to 4.5° per millimeter but this value can be easily tuned by varying the gradient profile of the initial titania coating. The capability of this gradient to provoke droplet motion on the surface is demonstrated in Figure 7e. The optical images were taken with the contact angle device. The sequence shows the displacement of a 4 μL water droplet in the direction where the film is less concentrated in m-SiO_2 and thus more hydrophilic. In addition, the presence of the wettability gradient induces the formation of an asymmetric profile in droplet shape that is clearly visible after 0.3 s. With respect to other techniques proposed to fabricate wetting gradients, our approach based on dip-coating gives several combined advantages. The process is well adapted to create controlled, "on-demand" wetting profile on large surfaces; the final ceramic coating is robust and, if polluted by organics, can be regenerated by thermal treatment at 400 °C. Compared to other processes involving nano/microstructuration, our approach permits preservation of the optical quality of the graded layers (as proved by the fact that ellipsometer measurements could be made). All these aspects are very important since such wettability gradients could be applied on transparent windows/solar cells for water harvesting or integrated in transparent pump-free microfluidic devices.

3. CONCLUSION

In this work, we describe a general and simple strategy to obtain graded films and to generate devices with controlled functionality gradients based on dip-coating process in acceleration mode. In the first part of the Article, we investigated the effect of the acceleration in the dip coating process. In particular, we highlighted the crucial roles played by the evaporation rate and by the viscosity on the fluid draining-induced film formation. We demonstrated that on-demand thickness profiles could be prepared. The approach was applied to fabricate graded films of several relevant materials, including sol−gel dense and mesoporous metal oxides, block copolymers, metal−organic framework colloids, and commercial photoresists. In the second part, we describe how dip-coating in acceleration mode can be used to induce controlled variation of properties including structural, optical, chemical, or wetting. The versatility of the process was demonstrated by several examples of unique graded functional devices. Through these examples, we demonstrate that the dip-coating process in acceleration mode permits one to increase the degree of complexity in device construction, promoting the development of graded systems to a wide range of domains such as in photonics, microfluidics, or water harvesting.

4. EXPERIMENTAL SECTION

4.1. Film Preparation. Mesoporous titania thin films were prepared from a solution composed of $TiCl_4$/F127/H_2O/EtOH with a respective molar ratio of 1:0.006:30:*x* (where *x* varied from 10 to 40).The final solution was obtained by dissolving the precursors $TiCl_4$ in ethanol and water followed by the addition of F127. In a similar way, dense silica thin films were obtained from a solution composed of TEOS/H_2O/HCl/EtOH with a respective molar ratio of 1:5:0.005:40. Polystyrene-*block*-polyethylene oxide (PS-*b*-PEO) copolymer solutions were composed of PS-*b*-PEO/EtOH/THF with a respective molar ratio of 0.04:80:20. ZIF-8 colloids were prepared from a solution of $Zn(NO_3)_2{\cdot}6H_2O$ (2.933 g, 9.87 mmol; 98% Sigma-Aldrich) in 200 mL of methanol (Aldrich, 99%) that was rapidly poured into a solution of 2-methylimidazole (6.489 g, 79.04 mmol; 99% Aldrich) in 200 mL of methanol under vigorous stirring at room temperature. After 1 h the nanocrystals were separated from the milky dispersion by centrifugation at 20 000 rpm for 15 min. To remove the excess of unreacted acid and zinc nitrate species, ZIF-8 nanoparticles were readily redispersed in absolute ethanol and centrifuged. The average nanocrystal size was evaluated by SEM to be equal to 35 nm as previously reported.[36] In the graded devices, dense titania thin films were prepared from a solution composed of $TiCl_4$/F127/H_2O/EtOH with a respective molar ratio of 1:0.0001:30:20, while mesoporous silica films were prepared from a solution of TEOS/F127/H_2O/HCl/EtOH with a respective molar ratio of 1:0.002:5:0005:41. The microfluidic pattern was obtained by conventional optical lithography by UV-exposure of the AZ photoresist for 1 min and by developing in a 0.15 M KOH solution. The pattern was replicated by pouring fluid PDMS (Bluesil RTV A+B) on the top; the system was heated at 70 °C for 12 h in order to allow solidification by cross-linking. After demolding, the patterned PDMS channel was covered by a flat silicon substrate on which a thin top PDMS layer was previously applied. The surface with wetting gradient was obtained by impregnation of a mesoporous titania layer with gradient of thickness prepared as above. The impregnation was perfomed by dip-coating at 2 mm s^{-1} the graded system into a solution composed of MTEOS/H_2O/HCl/EtOH with respective molar ratio of 1:30:0.005:160.

4.2. Characterization. Thickness and refractive index of optical films were assessed using ellipsometry investigation (variable angle spectroscopic ellipsometry (VASE) M-2000U Woollam spectroscopic ellipsometer) in the visible range at an incidence angle of 70°. In order to access the thickness profiles in a precise manner, we used a collimated beam spot with radius equal to 84 μm. To avoid possible film pollution due to extended exposure to environment, measurements were quickly conducted after thermal treatment. Ellipsometry was also used to collect transmission spectra between 350 and 1000 nm. Microscope images showing the film structure were collected using field-emission gun scanning electron microscopy (FEG-SEM, Hitachi SU7000 instrument). Fluorescence microscopy was used to evaluate the final thickness of the graded channel. The channel was filled with an aqueous solution containing fluorescein (0.01 M) and NH_4OH (0.1 M). Images were recorded with an Axis microscope (Examinen D1-Zeiss) at 10× magnification using a λ = 488 nm filter. The recorded fluorescence intensity as a function of the position was evaluated by image analysis. Different images were merged in order to obtain Figure 6c.

■ ASSOCIATED CONTENT

Ⓢ Supporting Information

Physicochemical characteristics of the model solution and schematic represatations of the process. This material is available free of charge via the Internet at http://pubs.acs.org/.

■ AUTHOR INFORMATION

Corresponding Author

*E-mail: david.grosso@upmc.fr.

Notes

The authors declare no competing financial interest.

■ ACKNOWLEDGMENTS

We thank David Montero for his support for electronic microscopy (Institut des Matériaux de Paris Centre FR2482). We acknowledge the financial support from CNano Region Ile-de-France and the Labex Matisse.

■ REFERENCES

(1) Ju, J.; Bai, H.; Zheng, Y.; Zhao, T.; Fang, R.; Jiang, L. A Multi-structural and Multi-functional Integrated Fog Collection System in Cactus. *Nat. Commun.* **2012**, *3*, 1247.

(2) Pierscionek, B. K.; Chan, D. Y. C. Refractive Index Gradient of Human Lenses. *Optom. Vis. Sci.* **1989**, *66*, 822−829.

(3) Genzer, J.; Bhat, R. R. Surface-Bound Soft Matter Gradients. *Langmuir* **2008**, *24*, 2294−2317.

(4) Koo, H.-J.; Waynant, K. V.; Zhang, C.; Haasch, R. T.; Braun, P. V. General Method for Forming Micrometer-Scale Lateral Chemical Gradients in Polymer Brushes. *Chem. Mater.* **2014**, *26*, 2678−2683.

(5) Chaudhury, M. K.; Whitesides, G. M. How to Make Water Run Uphill. *Science* **1992**, *256*, 1539−1541.

(6) Hernández, S. C.; Bennett, C. J. C.; Junkermeier, C. E.; Tsoi, S. D.; Bezares, F. J.; Stine, R.; Robinson, J. T.; Lock, E. H.; Boris, D. R.; Pate, B. D.; Caldwell, J. D.; Reinecke, T. L.; Sheehan, P. E.; Walton, S. G. Chemical Gradients on Graphene To Drive Droplet Motion. *ACS Nano* **2013**, *7*, 4746−4755.

(7) Yu, X.; Wang, Z.; Jiang, Y.; Zhang, X. Surface Gradient Material: From Superhydrophobicity to Superhydrophilicity. *Langmuir* **2006**, *22*, 4483−4486.

(8) Ye, F.; Cui, C.; Kirkeminde, A.; Dong, D.; Collinson, M. M.; Higgins, D. A. Fluorescence Spectroscopy Studies of Silica Film Polarity Gradients Prepared by Infusion-Withdrawal Dip-Coating. *Chem. Mater.* **2010**, *22*, 2970−2977.

(9) Kannan, B.; Higgins, D. A.; Collinson, M. M. Aminoalkoxysilane Reactivity in Surface Amine Gradients Prepared by Controlled-Rate Infusion. *Langmuir* **2012**, *28*, 16091−16098.

(10) Giri, D.; Hanks, C. N.; Collinson, M. M.; Higgins, D. A. Single-Molecule Spectroscopic Imaging Studies of Polarity Gradients Prepared by Infusion-Withdrawal Dip-Coating. *J. Phys. Chem. C* **2014**, *118*, 6423−6432.

(11) Kim, S.-H.; Jeong, W. C.; Hwang, H.; Yang, S.-M. Robust Chirped Photonic Crystals Created by Controlled Colloidal Diffusion. *Angew. Chem., Int. Ed.* **2011**, *50*, 11649−11653.
(12) Sommers, A. D.; Brest, T. J.; Eid, K. F. Topography-Based Surface Tension Gradients to Facilitate Water Droplet Movement on Laser-Etched Copper Substrates. *Langmuir* **2013**, *29*, 12043−12050.
(13) Shastry, A.; Case, M. J.; Böhringer, K. F. Directing Droplets Using Microstructured Surfaces. *Langmuir* **2006**, *22*, 6161−6167.
(14) Carreón-González, C. E.; De La Torre Medina, J. n.; Piraux, L.; Encinas, A. Electrodeposition Growth of Nanowire Arrays with Height Gradient Profiles for Microwave Device Applications. *Nano Lett.* **2011**, *11*, 2023−2027.
(15) Grosso, D. How to Exploit the Full Potential of the Dip-coating Process to Better Control Film Formation. *J. Mater. Chem.* **2011**, *21*, 17033−17038.
(16) Faustini, M.; Boissiere, C.; Nicole, L.; Grosso, D. From Chemical Solutions to Inorganic Nanostructured Materials: A Journey into Evaporation-Driven Processes. *Chem. Mater.* **2014**, *26*, 709−723.
(17) Faustini, M.; Louis, B.; Albouy, P. A.; Kuemmel, M.; Grosso, D. Preparation of Sol−Gel Films by Dip-Coating in Extreme Conditions. *J. Phys. Chem. C* **2010**, *114*, 7637−7645.
(18) Landau, L.; Levich, B. Dragging of a Liquid by a Moving Plate. *Acta Physicochim. URSS* **1942**, *17*, 42−54.
(19) Brinker, C. J.; Frye, G. C.; Hurd, A. J.; Ashley, C. S. Fundamentals of Sol-Gel Dip Coating. *Thin Solid Films* **1991**, *201*, 97−108.
(20) Le Berre, M.; Chen, Y.; Baigl, D. From Convective Assembly to Landau-Levich Deposition of Multilayered Phospholipid Films of Controlled Thickness. *Langmuir* **2009**, *25*, 2554−2557.
(21) Davis, R. L.; Jayaraman, S.; Chaikin, P. M.; Register, R. A. Creating Controlled Thickness Gradients in Polymer Thin Films via Flowcoating. *Langmuir* **2014**, *30*, 5637−5644.
(22) Crepaldi, E. L.; Soler-Illia, G. J. d. A. A.; Grosso, D.; Cagnol, F.; Ribot, F.; Sanchez, C. Controlled Formation of Highly Organized Mesoporous Titania Thin Films: From Mesostructured Hybrids to Mesoporous Nanoanatase TiO2. *J. Am. Chem. Soc.* **2003**, *125*, 9770−9786.
(23) Fuertes, M. C.; Colodrero, S.; Lozano, G.; Gonzalez-Elipe, A. R.; Grosso, D.; Boissiere, C.; Sanchez, C.; Soler-Illia, G.; Miguez, H. Sorption Properties of Mesoporous Multilayer Thin Films. *J. Phys. Chem. C* **2008**, *112*, 3157−3163.
(24) Soler-Illia, G. J. A. A.; Angelome, P. C.; Fuertes, M. C.; Grosso, D.; Boissiere, C. Critical Aspects in the Production of Periodically Ordered Mesoporous Titania Thin Films. *Nanoscale* **2012**, *4*, 2549−2566.
(25) Lancelle-Beltran, E.; Prené, P.; Boscher, C.; Belleville, P.; Buvat, P.; Lambert, S.; Guillet, F.; Boissière, C.; Grosso, D.; Sanchez, C. Nanostructured Hybrid Solar Cells Based on Self-Assembled Mesoporous Titania Thin Films. *Chem. Mater.* **2006**, *18*, 6152−6156.
(26) Sinturel, C.; Vayer, M.; Morris, M.; Hillmyer, M. A. Solvent Vapor Annealing of Block Polymer Thin Films. *Macromolecules* **2013**, *46*, 5399−5415.
(27) Faustini, M.; Nicole, L.; Boissiere, C.; Innocenzi, P.; Sanchez, C.; Grosso, D. Hydrophobic, Antireflective, Self-Cleaning, and Antifogging Sol-Gel Coatings: An Example of Multifunctional Nanostructured Materials for Photovoltaic Cells. *Chem. Mater.* **2010**, *22*, 4406−4413.
(28) Angelomé, P. C.; Fuertes, M. C.; Soler-Illia, G. J. A. A. Multifunctional, Multilayer, Multiscale: Integrative Synthesis of Complex Macroporous and Mesoporous Thin Films with Spatial Separation of Porosity and Function. *Adv. Mater.* **2006**, *18*, 2397−2402.
(29) Gates, B. D.; Xu, Q. B.; Stewart, M.; Ryan, D.; Willson, C. G.; Whitesides, G. M. New Approaches to Nanofabrication: Molding, Printing, and Other Techniques. *Chem. Rev.* **2005**, *105*, 1171−1196.
(30) Leng, J.; Salmon, J. B. Microfluidic Crystallization. *Lab Chip* **2009**, *9*, 24−34.
(31) Faustini, M.; Kim, J.; Jeong, G.-Y.; Kim, J. Y.; Moon, H. R.; Ahn, W.-S.; Kim, D.-P. Microfluidic Approach toward Continuous and Ultrafast Synthesis of Metal−Organic Framework Crystals and Hetero Structures in Confined Microdroplets. *J. Am. Chem. Soc.* **2013**, *135*, 14619−14626.
(32) Tan, Y. C.; Fisher, J. S.; Lee, A. I.; Cristini, V.; Lee, A. P. Design of Microfluidic Channel Geometries for the Control of Droplet Volume, Chemical Concentration, and Sorting. *Lab Chip* **2004**, *4*, 292−298.
(33) Faustini, M.; Capobianchi, A.; Varvaro, G.; Grosso, D. Highly Controlled Dip-Coating Deposition of fct FePt Nanoparticles from Layered Salt Precursor into Nanostructured Thin Films: An Easy Way To Tune Magnetic and Optical Properties. *Chem. Mater.* **2012**, *24*, 1072−1079.
(34) Faustini, M.; Vayer, M.; Marmiroli, B.; Hillmyer, M.; Amenitsch, H.; Sinturel, C.; Grosso, D. Bottom-up Approach toward Titanosilicate Mesoporous Pillared Planar Nanochannels for Nanofluidic Applications. *Chem. Mater.* **2010**, *22*, 5687−5694.
(35) Lepoutre, S.; Julian-Lopez, B.; Sanchez, C.; Amenitsch, H.; Linden, M.; Grosso, D. Nanocasted Mesoporous Nanocrystalline ZnO Thin Films. *J. Mater. Chem.* **2010**, *20*, 537−542.
(36) Demessence, A.; Boissiere, C.; Grosso, D.; Horcajada, P.; Serre, C.; Ferey, G.; Soler-Illia, G.; Sanchez, C. Adsorption Properties in High Optical Quality NanoZIF-8 Thin Films with Tunable Thickness. *J. Mater. Chem.* **2010**, *20*, 7676−7681.